Title

Effect of turbulence–chemistry interactions on chemical pathways for turbulent hydrogen–air premixed flames

Authors

Dasgupta, Debolina
Sun, Wenting
Day, Marc
et al.

Publication Date

2017-02-01

DOI

10.1016/j.combustflame.2016.09.029

Peer reviewed

Combustion and Flame 176 (2017) 191–201

Contents lists available at ScienceDirect

Combustion and Flame

journal homepage: www.elsevier.com/locate/combustflame

Effect of turbulence–chemistry interactions on chemical pathways for turbulent hydrogen–air premixed flames☆

Debolina Dasgupta[a,*], Wenting Sun[a], Marc Day[b], Tim Lieuwen[a]

[a] School of Aerospace Engineering, Georgia Institute of Technology, 270 Ferst Drive, Montgomery Knight Building 0150, Atlanta, GA 30332, USA
[b] Center for Computational Sciences and Engineering, Lawrence Berkeley National Laboratory, Berkeley, CA 94720, USA

ARTICLE INFO

Article history:
Received 12 May 2016
Revised 19 July 2016
Accepted 28 September 2016
Available online 11 November 2016

Keywords:
Premixed flames
Turbulent combustion
Turbulent–chemistry interactions

ABSTRACT

This paper considers the kinetic pathways of hydrogen oxidation in turbulent, premixed H_2–air flames. It assesses the relative roles of different reaction steps in H_2 oxidation relative to laminar flames, and the degree to which turbulence–chemistry interactions alters the well understood oxidation pathway that exist in laminar flames. This is done by analyzing the turbulent, lean ($\phi = 0.4$), H_2–air flame DNS database from Aspden et al. [17]. The relative roles of dominant reaction steps in heat release and radical formation/consumption are analyzed at different Karlovitz numbers and compared with laminar stretched flame calculations from counterflow flames and perfectly stirred reactors. It is found that both the progress variable conditioned and spatially integrated contributions of the dominant reactions remain qualitatively similar between a highly turbulent and a laminar unstretched flame. Larger changes, up to a factor of about two, occur in the relative roles of reactions with secondary influences on heat release and radical production/consumption. These results suggest that the kinetic routes through which H_2 is oxidized remain essentially constant between laminar, unstretched flames and high Karlovitz number flames.

1. Introduction

This paper considers the kinetic pathways of hydrogen (H_2) oxidation in turbulent, premixed H_2–air flames. The kinetics of hydrogen combustion in laminar, premixed flames are well established [1–3]. To illustrate, Fig. 1 depicts a network diagram for the production and consumption of different species and radicals involved in the oxidation of hydrogen to water (H_2O), as predicted by Li et al.'s [2] mechanism. This diagram considers the first generation (species directly forming water i.e. H, OH) and second generation(species indirectly forming water i.e. HO_2) species similar to path flux analysis [4] for reduction of chemical mechanisms. It can be seen, for example, most of the fuel (81%) directly forms water (81%) through the reaction, $H_2 + OH \rightarrow H_2O + H$. The rest of the fuel is indirectly converted to water through the H and OH radicals via different reactions such as $H + OH + M \rightarrow H_2O + M$, $HO_2 + OH \rightarrow H_2O + O_2$.

A key question motivating this study is whether this basic picture remains essentially the same in turbulent flames or is fundamentally altered. In other words, could the dominant reaction steps in a turbulent flame be substantively different than in a laminar flame? There are several mechanisms through which the relative contributions of different reactions could be altered in turbulent flames relative to laminar flames. First, tangential straining and curvature of scalar isosurfaces leads to flame stretch, κ. Flames are stretched by both hydrodynamic straining and curvature, as given by the expression below:

$$\kappa = K_S + s_d \mathbb{K}_C \tag{1}$$

where s_d is the displacement speed of the iso-surface at which the flame strain K_S and curvature $\mathbb{K}_C$ are defined. Stretch alters local temperatures and the relative concentrations of major and minor species [5]. Moreover, turbulent flames are highly stretched and curved.

However, many different types of stretch effects can be analyzed with laminar, steady state, stretched flames. Indeed, steady stretch effects on the flame structure and reaction pathways have been studied extensively, such as in opposed-flow flames [6,7]. Nonetheless, there are complications in application of these laminar, model configurations to turbulent flamelets. For example, it is known that strongly stretched flames respond differently to curvature and tangential strain, and turbulent flames can be subjected to different combinations of these. For example, taking the two components of curvature of an isosurface, $\mathbb{K}_C = \mathbb{k}_1 + \mathbb{k}_2$, a given isosurface can have curvatures that approach that of cylindrical or

☆ Based upon AIAA Paper #2016-1688, copyright held by authors.

* Corresponding author.
E-mail address: debolina.dasgupta@gatech.edu (D. Dasgupta).

http://dx.doi.org/10.1016/j.combustflame.2016.09.029
0010-2180/

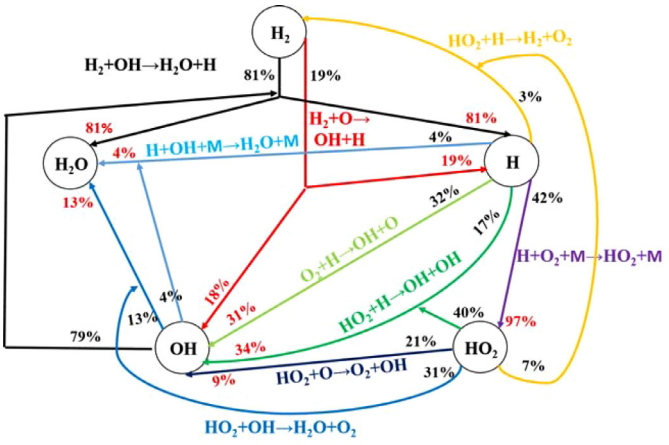

Fig. 1. Hydrogen pathway for water formation for unstretched laminar flames (black: % of production, red: % of consumption), as predicted by Li et al.'s mechanism [2]. (For interpretation of the references to colour in this figure legend, the reader is referred to the web version of this article.)

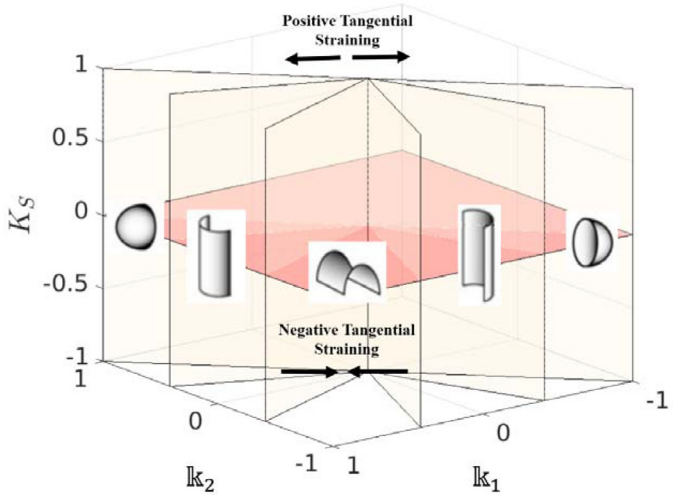

Fig. 2. Illustration of potential iso-surface curvature and stretch combinations.

spherical surfaces or, if they have opposite signs, a saddle point. In addition, the local tangential strain can be positive or negative. The three dimensional space afforded by the different $\mathbb{k}_1, \mathbb{k}_2, K_S$ combinations are illustrated pictorially in Fig. 2, showing, that ten (five different topological configurations, and two different stretching combinations) different stretched flame combinations are possible in a turbulent flame.

The solution spaces of turbulent flames may not uniformly occupy all regions in this volume. Studies suggest that curvature and strain are correlated with each other [8–10], but this correlation varies through the flame—e.g., Kim and Pitsch [11] showed that there was a negative curvature–strain correlation at low progress variable contours in the flamelet, and no correlation at values farther into the flamelet. Turbulent distortions of the flamelet introduce a large number of potential combinations and topologies for flame stretch, and while the flame response to stretch in some of these areas is well characterized (e.g., flat, tangentially strained flames), a systematic analysis of steady, laminar flames to different stretch levels does not yet appear to exist.

A second mechanism through which the relative contributions of different reactions could be altered in turbulent flames is due to unsteady kinetic and diffusive effects. We can define a chemical time and an associated Karlovitz number associated with the *i*th reaction as

$$Ka_i = \tau_{chem,i}\ \kappa \tag{2}$$

Different reactions have different characteristic chemical times and their instantaneous rates and relative roles in the overall oxidation and heat release pathway may be altered in cases where the response of one or more reactions to unsteady stretch is not quasi-steady, i.e., $Ka_i \sim O(1)$. In addition, even in cases where all reactions are quasi-steady, local radical concentrations may not be at quasi-steady values due to diffusive time lags. Again, these effects can and have been considered from model, laminar flamelet problems [5,12,13]. As such, referring back to Fig. 2, turbulent flames present a large number of possible combinations to unsteady stretch.

A third mechanism through which turbulence can modify the contributions of different reactions relative to laminar flames is through the "stirring" action of small scale eddies within the flamelet, introducing spatially differentiated convective transport of species along the flamelet.

There exists a large literature on the effects of turbulence on flame structure, and the reader is referred to Borghi [14], Peters [15], and Driscoll [16] for further discussion of this point. In addition, several prior studies have also analyzed the specific question of chemical pathways in turbulent flames. Aspden et al. [17] noted that in lean hydrogen/air turbulent premixed flames, regions of high curvature tend to have relatively low heat release in spite of having higher fuel consumption. This decorrelation between fuel consumption and heat release is due to the reactions $H + O_2 + M \rightarrow HO_2 + M$, $HO_2 + H \rightarrow OH + OH$ and $HO_2 + OH \rightarrow H_2O + O_2$, which do not involve H_2 (and hence fuel consumption). These are responsible for much of the heat released in regions of negative curvature. They divided the temperature range into two regions, above and below 992 K and integrated the heat released in each region separately. They noted a 7-fold increase in heat release in the low temperature region between $Ka = 1$ and $Ka = 36$ due to the three aforementioned reactions, and attribute this behavior to result from the enhanced radical pool at lower temperatures with increasing *Ka*.

Carlsson et al. [18] also observed similar modifications to heat release in their DNS studies of lean premixed methane/air and hydrogen/air flames. The reaction, $H + O_2 + M \rightarrow HO_2 + M$, has negligible heat release in low temperature regions in 1D laminar or low *Ka* turbulent flames. They argued that the time scale for the diffusion transport of H radicals is much smaller than the chemical time scale for this reaction; H radicals are found close to the high temperature regions where they are formed. However, increasing turbulence reduces the effective diffusion time scale, which can, thus, become comparable to the chemical time scale for the chain termination reaction. This scenario leads to a higher concentration of H radicals in low temperature regions. Day et al. [19] examined 2D DNS of H_2–CH_4–air turbulent flames. They noted three different regions of the flame front (a) intense burning regions with positive curvature, (b) weak burning regions with negative curvature (c) large scale flame folding regions (regions where H_2 consumption is zero but C_2 hydrocarbon concentrations are high). They investigated corresponding changes in C and C_2 kinetic pathways for each of these regions. The C pathway via CH_3O increased from 4.2% in region (a) to 7.7% in region (b) to 11.8% in region (c). The C_2 pathway shifted from 2.7% to 3.8% to 5.1% in regions (a), (b) and (c) respectively.

The objective of this paper is to further explore global changes in chemical pathways induced by turbulent mixing in lean premixed hydrogen/air combustion, and to compare these results with model laminar flame computations. Its key contribution to the literature is to analyze how different reaction steps contribute to heat release and radical production, and how these relative roles vary between model laminar flames/ PSR's, and turbulent flames

Table 1
Summary of DNS cases.

Case	u' (m/s)	u'/s_F	Ka_F
A	0.75	1.6	1
B	1.9	4.0	4
C	3.9	8.3	12
D	8.2	17	36

over a range of Karlovitz numbers. This is done by assessing these relative roles by spatially integrating across the flame, conditioning on specific turbulent flame progress variables, temperature isosurfaces, and topological flame features (e.g., spherical concave regions relative to saddle-points).

2. Numerical procedures

This paper analyses the DNS data set from Aspden et al. [17], which consists of a nominally one-dimensional, lean ($\phi = 0.4$), premixed hydrogen–air flame. The DNS solves low-Mach number reacting flow equations with mixture-averaged transport for molecular diffusion with no Soret, Dufour, gravity and radiative processes. Li et al.'s [2] kinetic mechanism, thermodynamic properties and transport coefficients of the H_2/O_2 system are used. This mechanism consists of 9 species and 21 reaction steps. The DNS utilizes reactant temperature $T^u = 298$ K at a pressure of 1 atm. A high aspect ratio domain (8:1:1) is used for the simulations with lateral periodic boundary conditions, free-slip fixed wall at the bottom and outflow at the top. A density-weighted forcing term in the momentum equations maintains the turbulence, with an integral length scale of $l/l_F = 4$, where l and l_F denote the integral length scale and freely-propagating flame length respectively. Four cases of increasing turbulence intensity (Karlovitz number = 1, 4, 12 and 36) are analyzed where Karlovitz number is defined as:

$$Ka_F{}^2 = \frac{u'^3}{s_F{}^3}\,\frac{l_F}{l} \tag{3}$$

Here u' is the turbulent rms velocity and s_F is the freely-propagating flame speed. For these cases, $s_F \approx 47$ cm/s and $l_F \approx 410\,\mu$m [17]. Note that the propagation speed of a thermodiffusively unstable, lean hydrogen flame is different from its laminar, unstretched value, S_{Lo}. We used the former values, following Aspden et al. [20], who argued that freely propagating flames provide a better normalization for hydrogen flames than the laminar, unstretched values. For reference $S_F/S_{Lo} \sim 2.1$ and $l_F/l_L = 0.6$. Table 1 summarizes these cases.

Figure 3 shows sample images of the 1144 K thermal isosurface for these four cases.

A reference isosurface is needed to associate the local curvature and stretch values, and the flame normal. Here, the reference isosurface is taken at the temperature of peak fuel consumption rate in a steady, unstretched flame at the same equivalence ratio, which has a value of $T_{ref} = 1144$ K. Spatial integration of reaction rates and species consumption rates are defined over volumes whose lateral surfaces are normal to this reference surface. The spatial integration procedure starts with a tessellation of the T_{ref} isosurface, and defines a local coordinate parallel to integral curves of the local temperature gradient, as shown in Fig. 4.

The reaction rate is integrated over the volume and normalized by the reference surface area to yield a line integrated average at

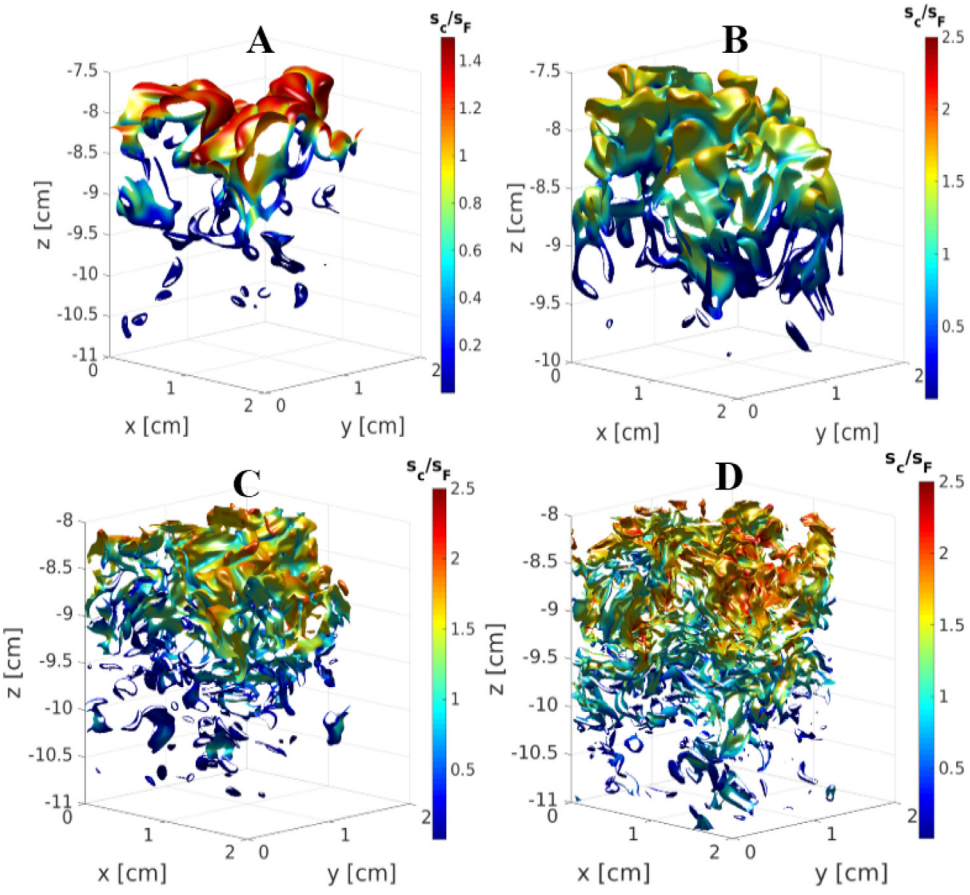

Fig. 3. Illustration of 1144 K temperature isosurfaces for four different Karlovitz number cases. The surfaces are colored by the consumption speed normalized by freely-propagating flame speed. (For interpretation of the references to colour in this figure legend, the reader is referred to the web version of this article.)

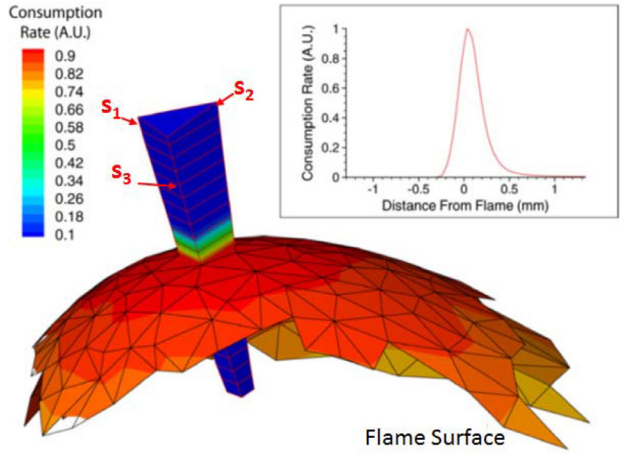

Fig. 4. Prism shaped volume, Ω, constructed using curves s_j locally normal to the temperature isotherms; the inset plot shows a typical variation of $\dot{\omega}_{H_2}$ along s_j [21].

each time instant:

$$\overline{RR_k}\left(\vec{x},t\right) = \frac{\int RR_k\left(\vec{x},t\right) d\Omega}{A_{ref}} \tag{4}$$

A_{ref} is the intersection area of the reference surface and the volume Ω. The average heat release rates and the H/OH/HO_2 radical consumption and production by each of the reactions can thus be calculated using these average reaction rates. The DNS data analyzed here is based upon a single time instant, extracted from the statistically stationary simulation results after the initial flame development transient phase.

The mean fuel consumption, $\overline{\dot{\omega}}_{H_2}$ can be calculated as shown in Eq. (4) by integrating $\dot{\omega}_{H_2}$ over the volume Ω. The direction of propagation, Z (shown in Fig. 3) is divided into 200 points between the lowest (Z_{min}) and the highest point (Z_{max}) (for example, −11 and −8 cm in Fig. 3D). The cumulative fuel consumption is then calculated along this direction and normalized by the total fuel consumption in the volume. A typical profile for the fuel consumption is shown in Fig. 5. We define a progress variable, $\bar{c}_i$, at a location, Z_i, as:

$$\bar{c}_i = \frac{\sum_{Z_i<Z<Z_{\max}} \overline{\dot{\omega}}_{H_2}}{\sum \overline{\dot{\omega}}_{H_2}} \tag{5}$$

The location, $\bar{c} = 0$, corresponds to unburnt reactants.

The heat release contribution of the individual reactions, $\overline{\dot{q}_k}$ and the rate of formation/consumption of species, i by reaction k, at a certain progress variable $\bar{c}_i$, at every point on the reference surface is defined as:

$$\overline{\dot{q}_k}(x,y)\big|_{\bar{c}_i} = \overline{RR_k}(x,y)\big|_{\bar{c}_i}\left(\Delta h_f^o\big|_{reac} - \Delta h_f^o\big|_{prod}\right) \tag{6}$$

$$\overline{\dot{\omega}_{i,k}}(x,y)\big|_{\bar{c}_i} = \overline{RR_k}(x,y)\big|_{\bar{c}_i}\left(\nu''_{i,k} - \nu'_{i,k}\right) \tag{7}$$

where a generalized reaction is written as $\nu'_{i,k}M_i \rightarrow \nu''_{i,k}M_i$. The reaction rate, $\overline{RR_k}(x,y)$ can be greater or less than zero. If $\overline{RR_k}(x,y) < 0$, then the reverse reaction from the mechanism is used for the analysis.

The area-weighted average heat release and the rate of formation/consumption of species at a certain progress variable $\bar{c}_i$, $\overline{\dot{q}_k}|_{\bar{c}_i}$ and $\overline{\dot{\omega}_{i,k}}|_{\bar{c}_i}$ can then be computed as:

$$\overline{\dot{q}_k}\big|_{\bar{c}_i} = \frac{\sum_{j=1}^{j=N} \overline{\dot{q}_k}(x,y)\big|_{\bar{c}_i} A_{ref,j}}{\sum_{j=1}^{j=N} A_{ref,j}} \tag{8}$$

$$\overline{\dot{\omega}_{i,k}}\big|_{\bar{c}_i} = \frac{\sum_{j=1}^{j=N} \overline{\dot{\omega}_{i,k}}(x,y)\big|_{\bar{c}_i} A_{ref,j}}{\sum_{j=1}^{j=N} A_{ref,j}} \tag{9}$$

where N is the number of points on the reference isosurface. A value of $\overline{\dot{\omega}_{i,k}}|_{\bar{c}_i} > 0$ implies that species, i is produced by reaction, k. We perform a separate accounting of the production and consumption of several key species below.

The net heat release and production of species, i at $\bar{c}_i$ is:

$$\overline{\dot{q}}\big|_{\bar{c}_i} = \sum_k \overline{\dot{q}_k}\big|_{\bar{c}_i} \tag{10}$$

The net production of species, i at $\bar{c}_i$ is given as:

$$\overline{\dot{\omega}_{i,p}}\big|_{\bar{c}_i} = \sum_k \overline{\dot{\omega}_{i,k}}\big|_{\bar{c}_i} \tag{11}$$

Here if the reaction k, forms species, i then $\overline{\dot{\omega}_{i,k}} > 0$ else $\overline{\dot{\omega}_{i,k}} = 0$. Similarly, the net consumption is given as:

$$\overline{\dot{\omega}_{i,c}}\big|_{\bar{c}_i} = \sum_k \overline{\dot{\omega}_{i,k}}\big|_{\bar{c}_i} \tag{12}$$

Here if the reaction, k consumes species, i then $\overline{\dot{\omega}_{i,k}} < 0$ else $\overline{\dot{\omega}_{i,k}} = 0$. The subscript p and c denote production and consumption respectively. The values obtained in Eqs. (10)–(12) are used for normalizing the values obtained in Eqs. (8) and (9)

For the global analysis, the heat release from the kth reaction across all progress variables (i.e. for the entire flame) is calculated as:

$$\overline{\dot{q}_k} = \sum_{0\le\bar{c}_i\le1} \overline{\dot{q}_k}\big|_{\bar{c}_i} \tag{13}$$

Similarly, the rate of formation/consumption of species, i by reaction k is calculated as:

$$\overline{\dot{\omega}_{i,k}} = \sum_{0\le\bar{c}_i\le1} \overline{\dot{\omega}_{i,k}}\big|_{\bar{c}_i} \tag{14}$$

The total global heat release is then obtained as:

$$\overline{\dot{q}} = \sum_k \overline{\dot{q}_k} \tag{15}$$

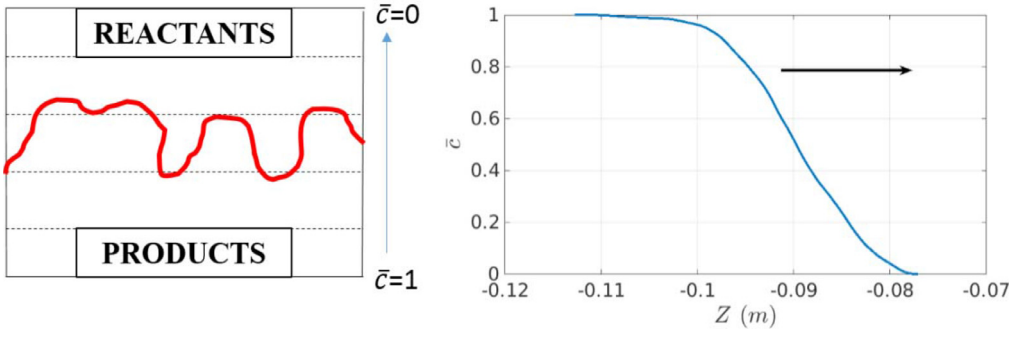

Fig. 5. Left: illustration of progress variable, $\bar{c}$. Right: mapping of physical space to progress variable. The arrows denote the direction of propagation.

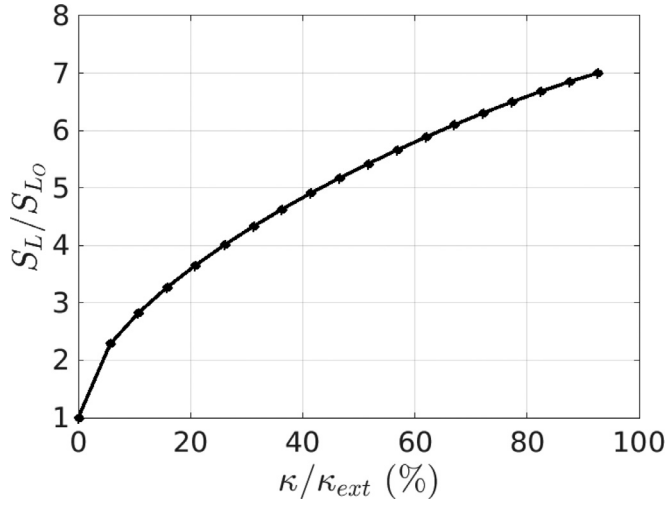

Fig. 6. Variation of laminar flame speed (normalized by the unstretched laminar flame speed) with stretch, calculated using OPPDIF for hydrogen–air flame at the same conditions and using the same kinetic mechanism as the DNS calculations.

The net production and consumption of species, i are given as:

$$\overline{\dot{\omega}_{i,p}} = \sum_k \overline{\dot{\omega}_{i,k}} \tag{16}$$

$$\overline{\dot{\omega}_{i,c}} = \sum_k \overline{\dot{\omega}_{i,k}} \tag{17}$$

In order to provide reference values for comparisons, calculations are also performed for the following three model reactor/flame configurations at the same inlet conditions as the DNS (1) steady unstretched flames using the PREMIX code (2) steady stretched, premixed flames using OPPDIF [22] code, and (3) perfectly stirred reactors using PSR [23]. Sample results from the OPPDIF calculation are shown in Fig. 6.

A typical maximum number of 8000 grid points was used to ensure convergence of individual OPPDIF runs with a value of 0.01 for adaptive grid control based on profile curvature and gradient (CURV and GRAD). The radial velocity is set to zero at the inlets. The stretch rate, κ, is given by the maximum value of $-du/dx$ between the inlet and the first minima in the axial velocity profile. The extinction stretch rate is given by κ_{ext} and equals 10,170 1/s.

Net heat release and reaction rates are computed from OPPDIF results by integrating the heat release and reaction rate profiles in the axial direction:

$$\bar{q}_k = \sum_{j=1}^{j=N} q_{k,j} dx_j, \quad \bar{q} = \sum_k \bar{q}_k$$

$$\overline{\dot{R}R_k} = \sum_{j=1}^{j=N} R\dot{R}_{k_j} dx_j \tag{18}$$

$\overline{\dot{\omega}_{i,k}}$ can be calculated from $\overline{\dot{R}R_k}$ as outlined in Eq. (7). $\overline{\dot{\omega}_{i,p}}$ and $\overline{\dot{\omega}_{i,c}}$ are computed similar to Eqs. (16) and (17).

The PSR is setup with the same inlet fuel/air composition and inlet temperature as DNS. It was run with different residence times, τ_{res}, down to values approaching extinction, given by $\tau_{ext} = 0.08$ ms.

3. Results

Different metrics can be used to assess the degree to which chemical pathways are altered in turbulent flames. These include (1) fraction of heat release rate associated with a given reaction, (2) fraction of species production/consumption associated with a given reaction, (3) mole fraction of species/radicals at a given progress variable. These metrics can also be calculated at a fixed point in space and time, spatially integrated, or conditioned on progress variables or topological features (e.g., positive or negative curvature). For this paper, we focus on the relative roles of different reactions in the overall heat release rate as well as production of critical radical intermediates as a metric.

3.1. Global characteristics

As a baseline, we consider laminar flame and PSR results first, considering both stretched and unstretched (denoted as the $\kappa = 0$ case) results. These results show how the overall heat release changes with stretch/residence time, as well as the relative roles of the different reactions steps. We will then compare these results to the turbulent flame DNS results. The dependence of the total heat release rate (i.e. spatially integrated across the flame) upon stretch is plotted in Fig. 7(a) for the symmetric, opposed flow premixed flame case (calculated from OPPDIF). The heat release is normalized by surface area and is calculated at the centerline. As expected, the heat release rate increases with stretch until very close to extinction. Figure 7(b) plots the total heat release for the turbulent case upon Karlovitz number, where $Ka = 0$ corresponds to the laminar unstretched value and is the same as the $\kappa = 0$ value in Fig. 7(a). The spatially integrated heat release for the turbulent cases is normalized by the area of the computational domain i.e. 1.64 cm × 1.64 cm. The figure shows the clear increase in volumetric heat release with turbulence intensity. This increase in volumetric heat release is due to increases in surface area as well as burning rate per unit area (as quantified by the stretch factor). The rest of the figures in this paper will be normalized by these spatially integrated heat release rate values at the same stretch rate or residence time (for the laminar cases), or Karlovitz number (for the turbulent case).

Figure 8(a) plots the heat release (normalized by the total heat release for each case) associated with the given reactions as a function of normalized stretch rate, $\kappa/\kappa_{\text{ext}}$ and normalized residence time, $\tau_{\text{ext}}/\tau_{\text{res}}$, for the laminar flame reference cases. Results are shown for the largest magnitude exothermic and endothermic reactions (the other reaction steps that are not shown contribute an additional ~10% of the total heat release). The figure shows that $H + O_2(+M) \rightarrow HO_2(+M)$ is the dominant heat release reaction and that its relative importance changes only modestly with stretch, there being about an 11% difference from its unstretched value and its value at $\kappa/\kappa_{\text{ext}} = 0.4$. Note also the striking similarity of the PSR results with the stretched flamelet calculation. Similarly, the next two most important reactions are $H_2 + OH \rightarrow H_2O + H$ and $H + OH + M \rightarrow H_2O + M$, showing maximum changes of 10 and 120% respectively. This latter reaction has the largest fractional change of relative heat release of all these reactions. In general, the PSR results are quite similar to the OPPDIF results for all the reactions, with a maximum deviation of ~20% for the range of residence times calculated.

Figure 8(b) shows the same analysis for the turbulent flames (where $Ka = 0$ denotes the laminar, unstretched value). Turning to the individual reactions and comparing reactions side by side with the laminar results, note the strong similarity in both the relative significance of the different reactions, as well as their quantitative contributions to the heat release. In particular, the two exothermic reactions, $H + O_2(+M) \rightarrow HO_2(+M)$ and $H_2 + OH \rightarrow H_2O + H$, are dominant in the laminar and turbulent case. There is some shift in relative significance of the $HO_2 + OH \rightarrow H_2O + O_2$, $HO_2 + O \rightarrow O_2 + OH$ and $H + OH + M \rightarrow H_2O + M$ reactions, mirroring the laminar results. The biggest change in relative roles with Ka are the $H + OH + M \rightarrow H_2O + M$ and $HO_2 + H \rightarrow OH + OH$ reactions.

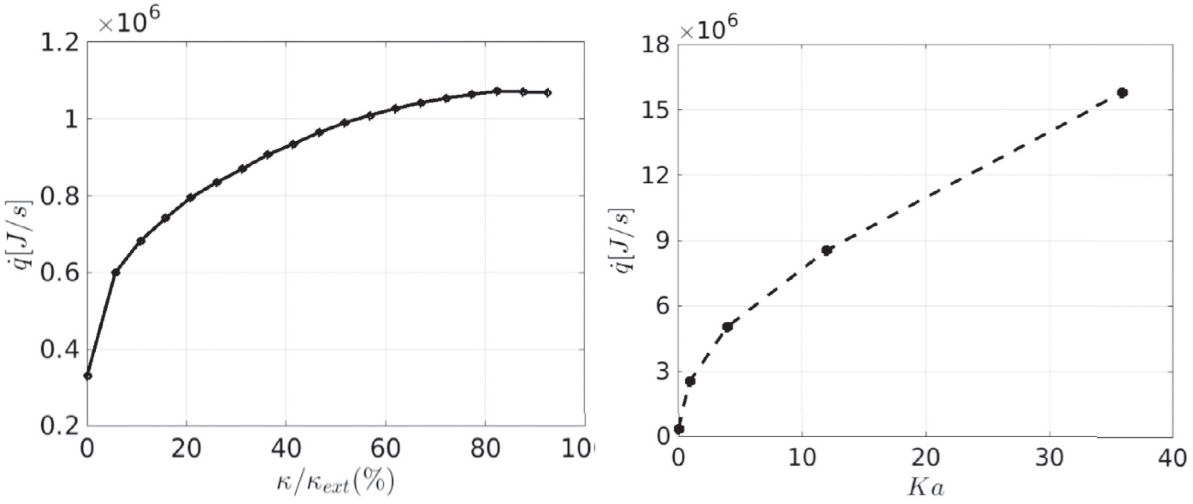

Fig. 7. Dependence of total heat release upon (a) stretch rate for laminar opposed flow configuration, and (b) Karlovitz number for the turbulent case. Heat release results are normalized by a reference surface area described in the text.

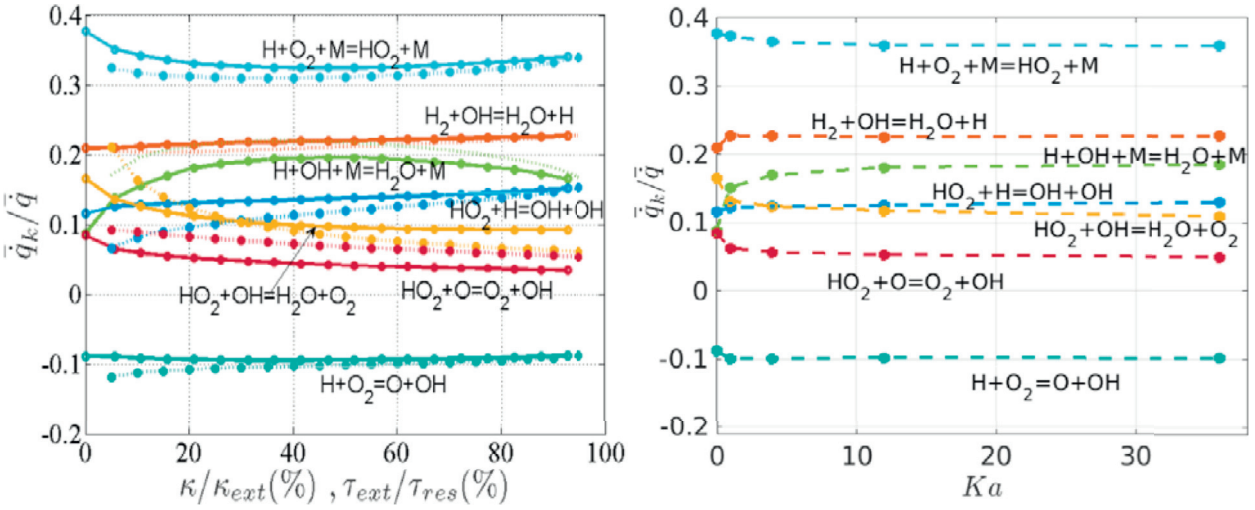

Fig. 8. Dependence of fractional heat release associated with different reactions upon (a) stretch (OPPDIF, solid line) and residence time (PSR, dotted line) and (b) Karlovitz number (DNS).

We next consider the relative roles of different reactions in producing reaction intermediates, focusing on H, OH, and HO_2 production. The integrated reaction rates are obtained as shown in Eqs. (4) and (18) for DNS and OPPDIF respectively. The consumption/production of a radical/species can then be calculated using the stoichiometric coefficients of the reaction as shown in Eq. (7). This consumption (or production) of a radical by a given reaction is normalized by the total consumption (or production) of this radical by all reactions as given by Eqs. (16) and (17).

Figure 9 shows the consumption/production of these radicals from DNS and OPPDIF. The consumption of H (shown in Fig. 9(a)) is dominated by the reaction $H + O_2 + M \rightarrow HO_2 + M$ and the trend resembles the heat release plot shown earlier of the same reaction. There is a change of ∼16% from the unstretched value to $\kappa/\kappa_{ext} = 0.4$ for the OPPDIF case and ∼14% change from $Ka = 0$ to $Ka = 36$ for the DNS. The next two dominant consumers of the H radical are $H + O_2 \rightarrow O + OH$ and $HO_2 + H \rightarrow OH + OH$. These are nearly insensitive to changes in stretch with maximum changes of 10% and 16%, respectively, over the entire range of stretch. The DNS shows even lower sensitivity of increasing turbulence with ∼3% and ∼5% changes in the consumption between $Ka = 1$ and $Ka = 36$. The reaction $H + OH + M \rightarrow H_2O + M$ shows the maximum change with stretch and Karlovitz number. The H consumption by this reaction almost doubles relative to its laminar unstretched value, similar to the heat release results for this reaction.

The reaction $HO_2 + H \rightarrow OH + OH$ produces the maximum OH (shown in Fig. 9(b)). The OH production rate increases with increasing κ and Ka demonstrating a change of ∼20% and ∼8% between the unstretched laminar value and $\kappa/\kappa_{ext} = 0.97$ for the stretched flames and $Ka = 36$ for the turbulent flames respectively. The production of OH by the reactions $H + O_2 \rightarrow O + OH$, $O + H_2 \rightarrow H + OH$, $HO_2 + O \rightarrow O_2 + OH$ and $O + H_2O \rightarrow OH + OH$ varies by 3%, 14%, 40% and 100% respectively for the entire range of stretch. The change is high for $O + H_2O \rightarrow OH + OH$ because this reaction reverses its direction for higher stretch values and thus, OH is consumed and not produced. However, these reactions show negligible changes from $Ka = 1$ to $Ka = 36$.

HO_2 consumption shows some significant changes with stretch and turbulence as demonstrated in Fig. 9(c). The dominant consumer of HO_2 is $HO_2 + H \rightarrow OH + OH$. The HO_2 consumption is augmented by 50% and 32% with increasing κ and Ka respectively. This consumption reduces by ∼33% and ∼50% for $HO_2 + OH \rightarrow H_2O + O_2$ and $HO_2 + O \rightarrow OH + O_2$ respectively from $\kappa/\kappa_{ext} = 0$ and $\kappa/\kappa_{ext} = 0.97$. The reduction is ∼25% and

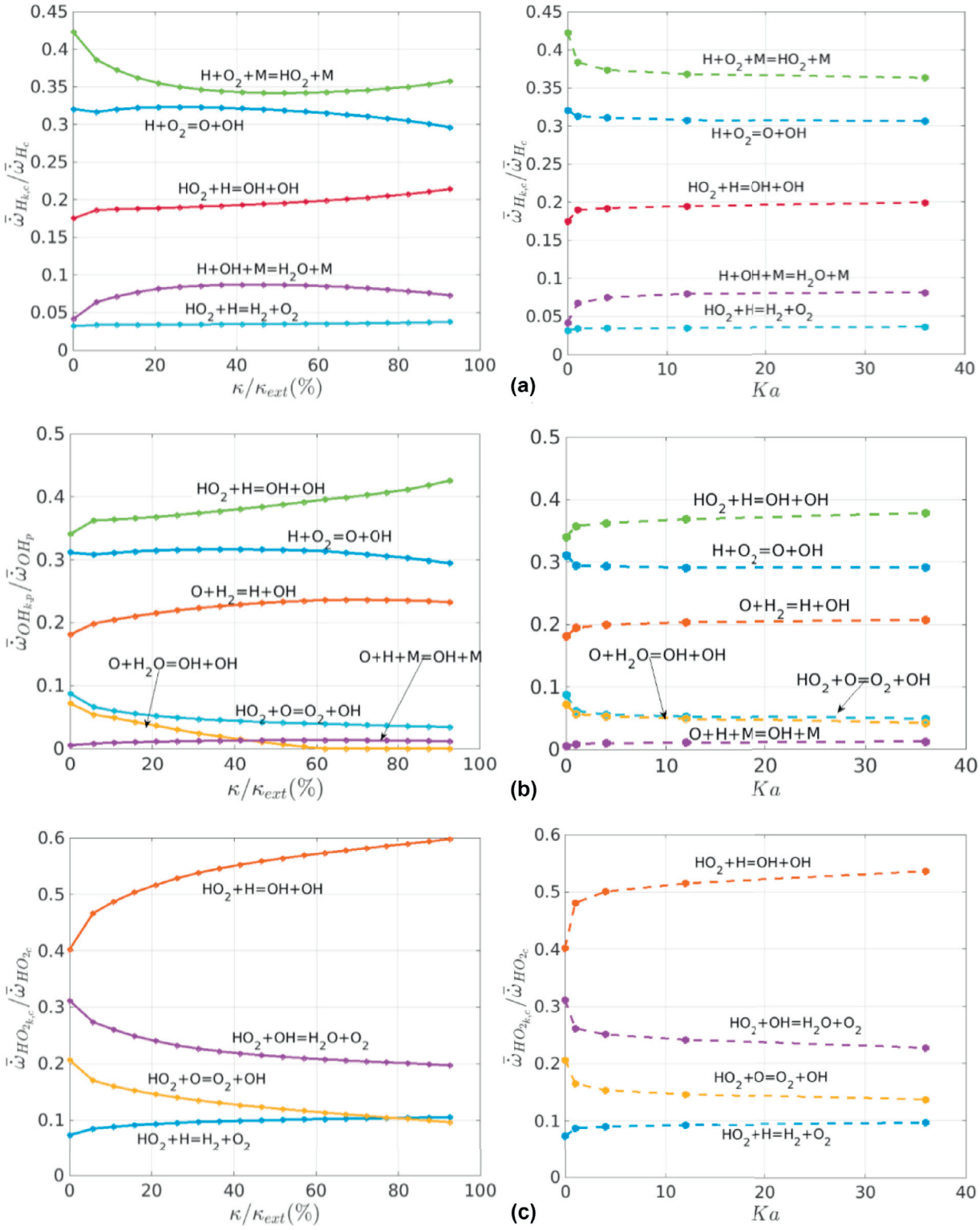

Fig. 9. Dependence of normalized (a) H consumption (b) OH production (c) HO_2 consumption by different reactions upon κ (left) and Ka (right).

~40% respectively from $Ka = 0$ to $Ka = 36$. It can be observed that the consumption of HO_2 by $HO_2 + H \rightarrow OH + OH$ increases. This chain branching reaction suppresses the chain termination reaction $HO_2 + OH \rightarrow H_2O + O_2$ and chain propagation reaction $HO_2 + O \rightarrow O_2 + OH$.

From these results, it is clear that the strong turbulence has little effect on the integrated chemical pathways in these lean-hydrogen flames. While there are some quantitative shifts, these differences are quite modest, particularly for the dominant reactions. However, these results are spatially integrated, and hence integrated over the entire temperature range. Temperature conditioned results are further discussed in Appendix A, but these results similarly show only modest changes.

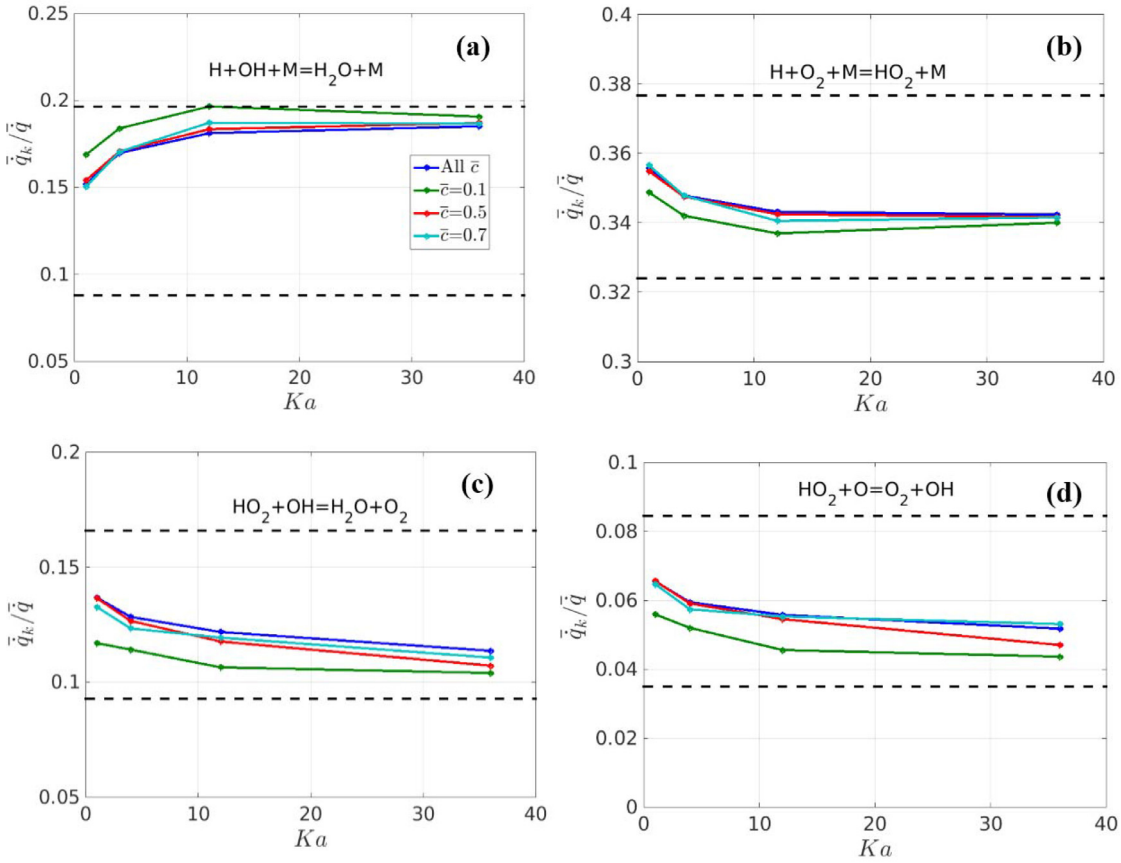

Fig. 10. Progress variable conditioned heat release for (a) $H + OH + M \rightarrow H_2O + M$ (b) $H + O_2 + M \rightarrow HO_2 + M$ (c) $HO_2 + OH \rightarrow H_2O + O_2$ (d) $HO_2 + O \rightarrow O_2 + OH$ (blue: all $\bar{c}$, green: $\bar{c} = 0.1$, red: $\bar{c} = 0.5$, cyan: $\bar{c} = 0.7$). Dashed horizontal lines denote range of values from OPPDIF calculations. (For interpretation of the references to colour in this figure legend, the reader is referred to the web version of this article.)

There is some possibility that more substantive local changes in reaction pathways may be occurring that do not manifest themselves strongly when averaged over the entire flame. For this reason, the next section considers more localized measures of the chemical pathways.

3.2. Progress variable conditioned results

This section considers similar metrics as the previous one, but focuses on spatial integrals between specific progress variables. Low progress variable values will necessarily be associated with more positively curved flame segments, due to their proximity to the leading edge of the front. As such, systematic differences in averaged stretch rates and curvature exist at different progress variables. Additional related results are shown in Appendix B, which shows results specifically conditioned on topological features.

We consider first the heat release. The relative contributions of different reactions are calculated by taking the area weighted average of the heat release given by Eq. (8) normalized by the total heat release given by Eq. (10). Progress variable conditioned heat release for some selected reactions are shown in Fig. 10— the blue line shows the same spatially integrated value shown in Fig. 8, while the green, red and cyan lines show $0.095 \leq \bar{c} \leq 0.105$, $0.495 \leq \bar{c} \leq 0.505$ and $0.695 \leq \bar{c} \leq 0.705$ respectively.

Again, quantitative differences exist, but they are modest. Moreover, the results conditioned on $\bar{c} = 0.5$ and 0.7 are quite close to the spatially averaged ones. The biggest differences occur at the leading edge of the brush, $\bar{c} = 0.1$. The dashed lines in the figures represent the OPPDIF bounds for these reactions, showing significantly larger ranges for the laminar, stretched flame calculations. Figures 11 and 12 show corresponding plots for the H and OH radical, also showing little change.

4. Conclusions

This paper discusses modifications to the chemical pathways of lean premixed hydrogen flames due to turbulence. The results are compared with counterflow flames and perfectly stirred reactors. It is found that the spatially integrated contributions of several key reactions to heat release, as well as H, OH, and HO_2 consumption, remain qualitatively similar between a highly turbulent and a steady unstretched flame configurations. For example, the contribution of the dominant exothermic reaction, $H + O_2 + M \rightarrow HO_2 + M$, to the heat release changes by about 20% between the unstretched, laminar flame and the $Ka = 36$ turbulent flame. The importance of the $H + OH + M \rightarrow H_2O + M$ reaction roughly doubles, which is a substantial effect, but its overall contribution to the heat release is only 1/2 to 1/3 of the most exothermic reaction. Similarly, the contribution of $HO_2 + OH \rightarrow H_2O + H$ to heat release reduces by ~45% from the steady unstretched values. This reaction, however, contributes only 1/4th of heat release of the most exothermic reaction. The dominant heat release reaction is also the dominant consumer of the H radical. However it shows a decreased consumption from the laminar unstretched case to the $Ka = 36$ case. The most significant change between the steady and turbulent cases is associated with the HO_2 consumption by the reaction $HO_2 + H \rightarrow OH + OH$, showing an increase by 40%. Its heat release shows minimal changes with increasing *Ka*.

Similarly, analysis of the chemical pathways for progress-variable-conditioned results showed strong similarities between

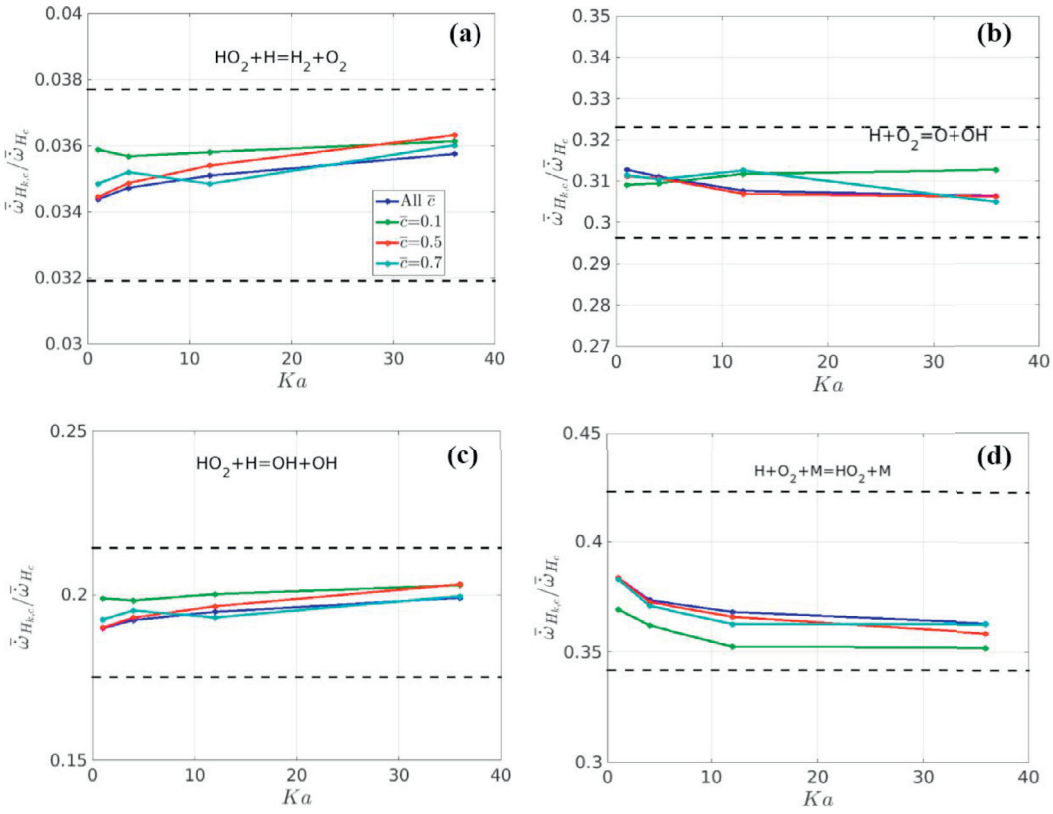

Fig. 11. Progress variable conditioned H consumption for (a) $HO_2 + H \rightarrow OH + OH$ (b) $H + O_2 \rightarrow O + OH$ (c) $HO_2 + H \rightarrow H_2 + O_2$ (d) $H + O_2 + M \rightarrow HO_2 + M$ (blue: all $\bar{c}$, green: $\bar{c} = 0.1$, red: $\bar{c} = 0.5$, cyan: $\bar{c} = 0.7$). Dashed horizontal lines denote range of values from OPPDIF calculations. (For interpretation of the references to colour in this figure legend, the reader is referred to the web version of this article.)

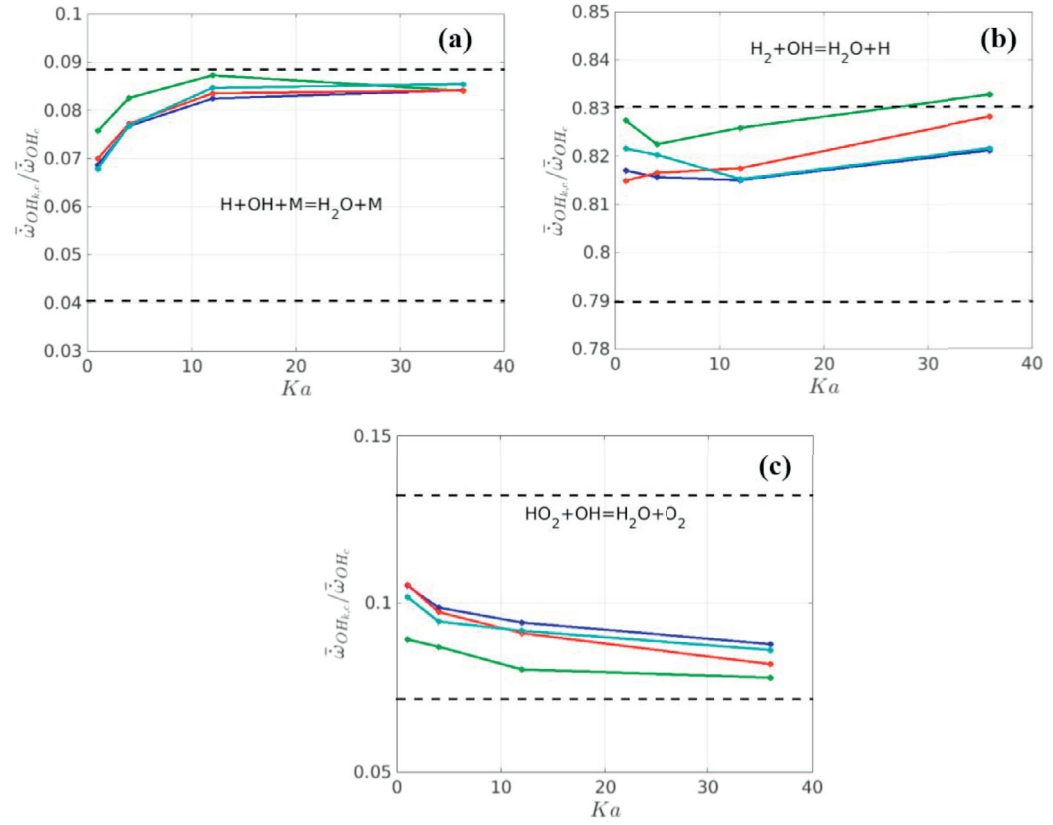

Fig. 12. Progress variable conditioned OH consumption for (a) $H + OH + M \rightarrow H_2O + M$ (b) $H_2 + OH \rightarrow H_2O + H$ (c) $HO_2 + OH \rightarrow H_2O + O_2$ (blue: all $\bar{c}$, green: $\bar{c} = 0.1$, red: $\bar{c} = 0.5$, cyan: $\bar{c} = 0.7$). Dashed horizontal lines denote range of values from OPPDIF calculations. (For interpretation of the references to colour in this figure legend, the reader is referred to the web version of this article.)

the steady unstretched cases and turbulent cases. The largest differences are seen near the leading edge of the brush, at $\tilde{c} = 0.1$, but even here the relative importance of the dominant exothermic reaction changes by 5% from $Ka = 1$ to $Ka = 36$.

The key implication of this work is that the kinetics of highly turbulent, lean premixed hydrogen–air flames is not markedly different from their steady, unstretched 1D counterparts. Ongoing work will consider similar questions for more complex fuels.

Appendix A. Temperature conditioning

This appendix discusses the relative contributions of the different reaction steps to heat release at a given temperature. This temperature conditioning was analyzed in order to determine if the results shown in the text, by virtue of being integrated quantities, smooth out potential changes in relative roles of different reactions within the flamelet. For example, it is possible that radical concentrations at a given isotherm change as one moves from laminar flames towards more distributed reactions at high Karlovitz numbers.

The variation of heat released by the dominant reactions at the specific temperatures of 500 K, 800 K, 1000 K, 1200 K, and 1400 K is shown in Fig. A1. The strong dependence of the reaction pathways on temperature is obvious. For example, $H + O_2 + M \rightarrow HO_2 + M$ is primarily a low-temperature region reaction and its primary contribution to heat release occurs at lower temperatures, and decreases by a factor of ~1.7 from 500 K to 1400 K. Similarly, the dominant heat release reaction shifts from $H + O_2 + M \rightarrow HO_2 + M$ to $H_2 + OH \rightarrow H_2O + H$ for temperatures above 1200 K. Nonetheless, these results show similarly modest changes in temperature-conditioned heat release contributions with Karlovitz number.

Appendix B. Curvature conditioning

This appendix shows how the role of different reactions vary with topological features. Figure 2 shows five different topological regions (concave/convex spherical elements, concave/convex cylindrical elements, and saddle points) conditioned on the two principal components of curvature, $\mathbb{k}_1$ and $\mathbb{k}_2$. The fraction of heat release associated with the dominant reactions, conditioned on these five regions is shown in Fig. B1. Burning rates are enhanced for lean H_2–air flames, and so the dominant heat release occurs in the spherical positively stretched elements, followed by positively stretched cylindrical elements, saddle points, then negatively stretched cylindrical elements, with the least heat release coming from negatively stretched spherical elements. This general trend would be expected, but it is interesting how the differences in relative contributions diminish with increasing Karlovitz number. For example, the contribution of positively stretched spherical elements drops by ~11% for $H + OH + M \rightarrow H_2O + M$, ~20% for $H + O_2 + M \rightarrow HO_2 + M$ and $H_2 + OH \rightarrow H_2O + H$ between Ka = 0 and 36. The relative contributions of the negatively curved

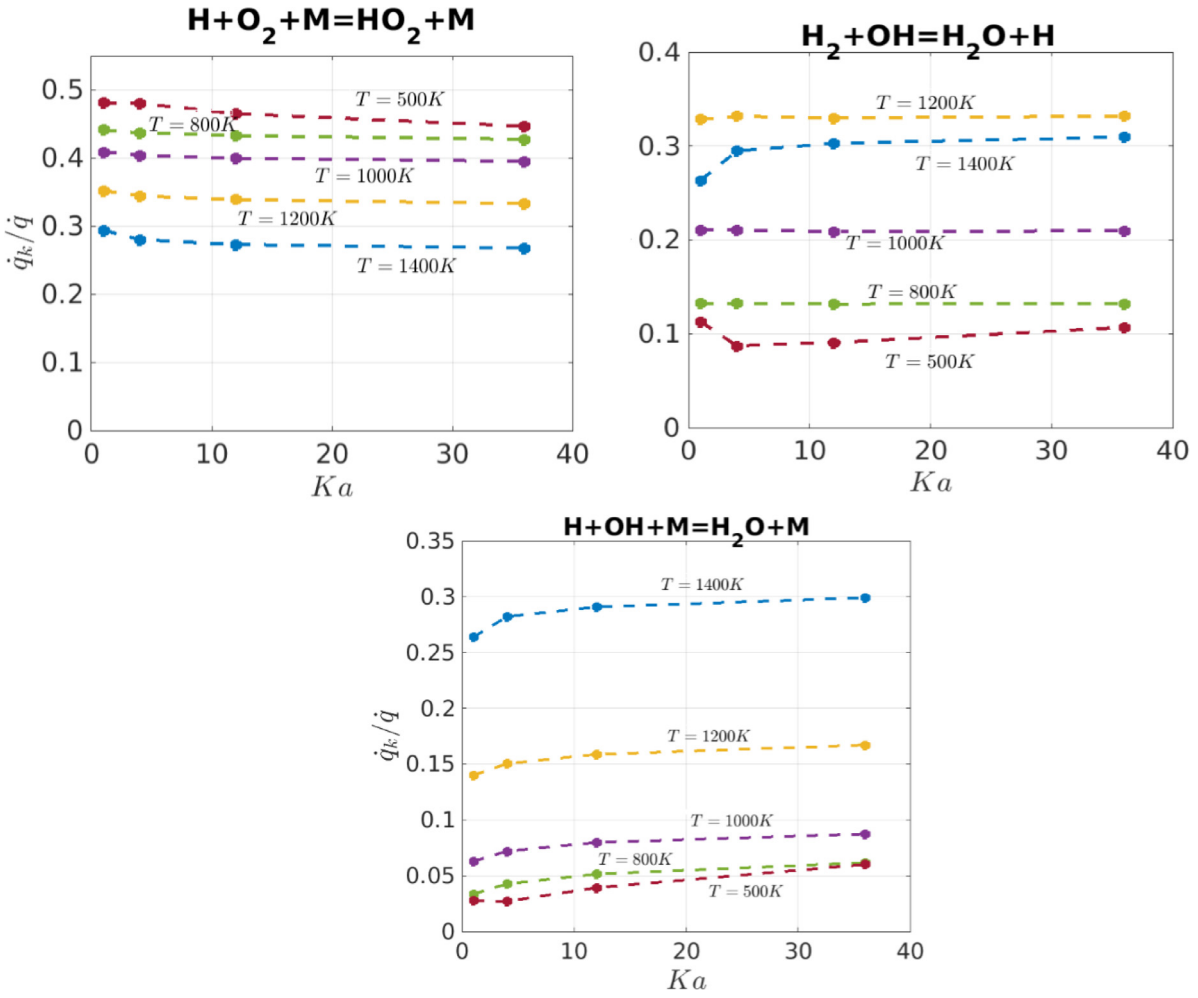

Fig. A1. Dependence of the normalized heat released by a reaction, at different temperatures, upon *Ka*. The heat released by the reaction (at a given temperature) is normalized by the total heat released at the given *Ka* at that temperature.

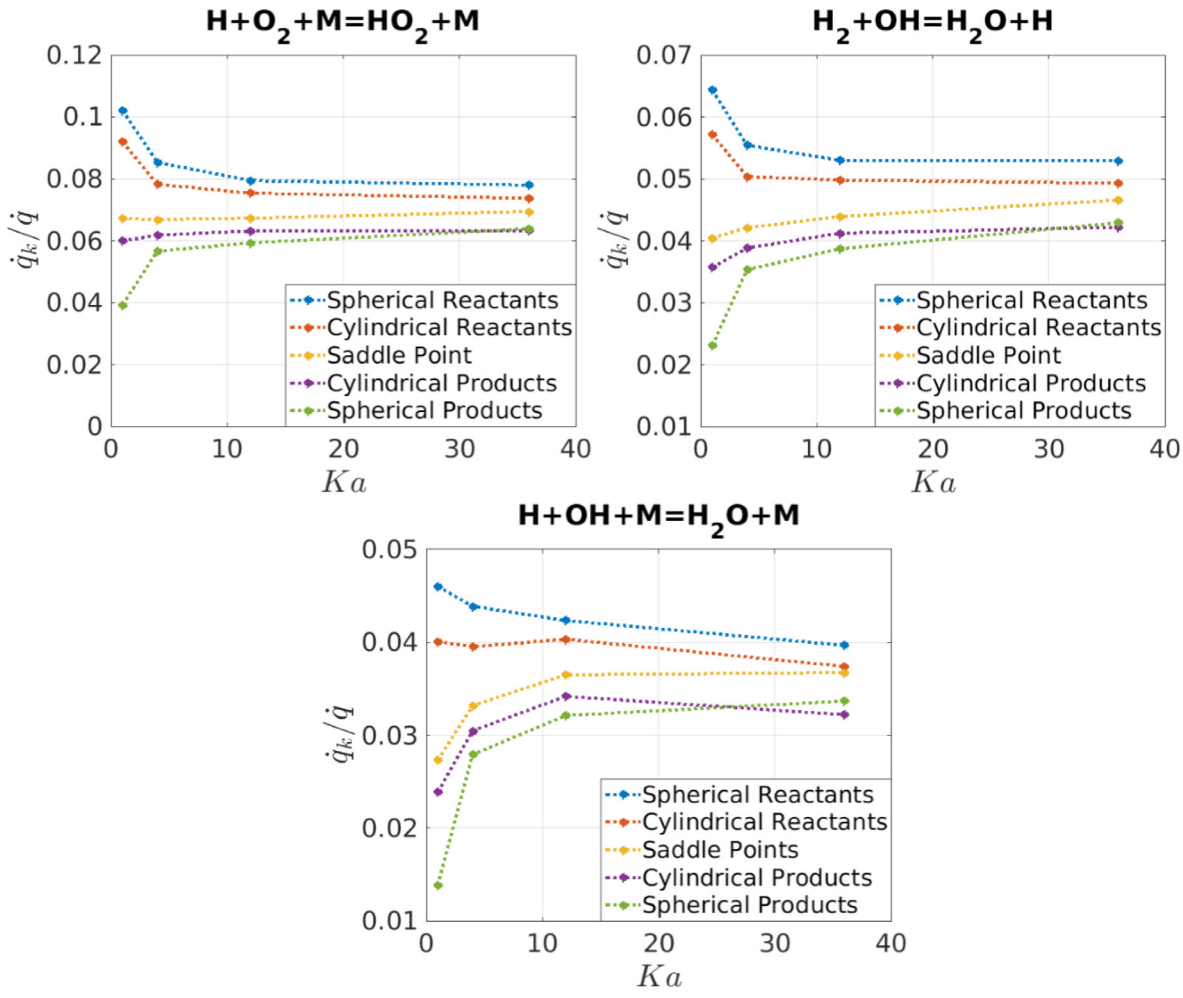

Fig. B1. Dependence of the fractional heat release of a given reaction in each of the five topological elements upon *Ka*. The heat released by a given reaction within an element is normalized by the total heat released at the given *Ka*.

spherical elements increase by ∼200% from Ka = 1 to Ka = 36 for $H + OH + M \rightarrow H_2O + M$, ∼50% for $H + O_2 + M \rightarrow HO_2 + M$ and ∼90% for $H_2 + OH \rightarrow H_2O + H$. This is likely an unsteady effect, as the burning rate sensitivity to stretch decreases with increasing frequency of the stretch fluctuations.

References

[1] I. Glassman, Combustion, Academic Press Inc., 1987.
[2] J. Li, Z. Zhao, A. Kazakov, F.L. Dryer, An updated comprehensive kinetic model of hydrogen combustion, Int. J. Chem. Kinet. 36 (2004) 566–575.
[3] M.P. Burke, M. Chaos, Y. Ju, F.L. Dryer, S.J. Klippenstein, Comprehensive H_2/O_2 kinetic model for high-pressure combustion, Int. J. Chem. Kinet. 44 (2012) 444–474.
[4] W. Sun, Z. Chen, X. Gou, Y. Ju, A path flux analysis method for the reduction of detailed chemical kinetic mechanisms, Combust. Flame 157 (2010) 1298–1307.
[5] C.K. Law, Combustion physics, Cambridge University Press, New York, 2006.
[6] C.K. Law, Dynamics of stretched flames, Symp. (Int.) Combust. 22 (1988) 1381–1402.
[7] C.K. Law, C.J. Sung, Structure, aerodynamics, and geometry of premixed flamelets, Prog. Energy Combust. Sci. 26 (2000) 459–505.
[8] N. Chakraborty, S. Cant, Unsteady effects of strain rate and curvature on turbulent premixed flames in an inflow–outflow configuration, Combust. Flame 137 (2004) 129–147.
[9] D.C. Haworth, T. Poinsot, Numerical simulations of Lewis number effects in turbulent premixed flames, J. Fluid Mech. 244 (1992) 405–436.
[10] N. Chakraborty, R.S. Cant, Effects of strain rate and curvature on surface density function transport in turbulent premixed flames in the thin reaction zones regime, Phys. Fluids 17 (2005) 065108.
[11] S.H. Kim, H. Pitsch, Scalar gradient and small-scale structure in turbulent premixed combustion, Phys. Fluids 19 (2007) 115104.
[12] H.G. Im, J.H. Chen, Effects of flow transients on the burning velocity of laminar hydrogen/air premixed flames, Proc. Combust. Inst. 28 (2000) 1833–1840.
[13] E.J. Welle, W.L. Roberts, C.D. Carter, J.M. Donbar, The response of a propane–air counter-flow diffusion flame subjected to a transient flow field, Combust. Flame 135 (2003) 285–297.
[14] R. Borghi, On the structure and morphology of turbulent premixed flames, in: C. Casci (Ed.), Recent Advances in the Aerospace Sciences, Plenum, New York, 1985, pp. 117–138.
[15] N. Peters, Laminar flamelet concepts in turbulent combustion, Symp. (Int.) Combust. (1986) 1231–1250.
[16] J.F. Driscoll, Turbulent premixed combustion: flamelet structure and its effect on turbulent burning velocities, Prog. Energy Combust. Sci. 34 (2008) 91–134.
[17] A.J. Aspden, M.S. Day, J.B. Bell, Turbulence–chemistry interaction in lean premixed hydrogen combustion, Proc. Combust. Inst. 35 (2015) 1321–1329.
[18] H. Carlsson, R. Yu, X.-S. Bai, Direct numerical simulation of lean premixed CH_4/air and H_2/air flames at high Karlovitz numbers, Int. J. Hydrogen Energy 39 (2014) 20216–20232.
[19] M.S. Day, X. Gao, J.B. Bell, Properties of lean turbulent methane–air flames with significant hydrogen addition, Proc. Combust. Inst. 33 (2011) 1601–1608.
[20] A.J. Aspden, M.S. Day, J.B. Bell, Characterization of low Lewis number flames, Proc. Combust. Inst. 33 (2011) 1463–1471.
[21] M. Day, J. Bell, P.T. Bremer, V. Pascucci, V. Beckner, M. Lijewski, Turbulence effects on cellular burning structures in lean premixed hydrogen flames, Combust. Flame 156 (2009) 1035–1045.
[22] A.E. Lutz, R.J. Kee, J.F. Grcar, F.M. Rupley, OPPDIF: a Fortran program for computing opposed-flow diffusion flames, Sandia National Laboratories, Livermore, CA, 1996.
[23] P. Glarborg, R.J. Kee, J.F. Grear, J.A. Miller, PSR: a FORTRAN program for modelling well-stirred reactors, Sandia National Laboratories, Livermore, CA, 1986.